Title: Direct Observation of the Pressure-Induced Structural Variation in Gold Nanoclusters and the Correlated Optical Response

Authors: Qi Li[1*], Charles J. Zeman IV[2], Bora Kalkan[3,4], Kristin Kirschbaum[5], Christopher G. Gianopoulos[5], Abhinav Parakh[6], David Doan[1], Andrew C. Lee[6], John Kulikowski[1], George C. Schatz[2], Guoyin Shen[7], Martin Kunz[4], X. Wendy Gu[1*]

Affiliations:

[1]Mechanical Engineering, Stanford University, Stanford, California 94305, United States
[2]Department of Chemistry, Northwestern University, Evanston, Illinois 60208, United States
[3]Earth and Planetary Sciences Department, University of California, Santa Cruz, CA, 95064, USA
[4]Advanced Light Source, Lawrence Berkeley National Lab, Berkeley 94720, United States
[5]College of Natural Sciences and Mathematics, University of Toledo, Toledo, Ohio 43606, United States
[6]Materials Science and Engineering, Stanford University, Stanford, California 94305, United States
[7]High Pressure Collaborative Access Team, X-ray Science Division, Argonne National Laboratory, Argonne, Illinois 60439, United States

Corresponding Authors: Qi Li qilistan@stanford.edu and X. Wendy Gu xwgu@stanford.edu

Abstract: The ability to gradually modify the atomic structures of nanomaterials and directly identify such structural vibration is important in nanoscience research. Here, we present the first example of a high-pressure single-crystal X-ray diffraction analysis of atomically precise metal nanoclusters. The pressure-dependent, sub-angstrom structural evolution of an ultrasmall gold nanoparticle, $Au_{25}S_{18}$, has been directly identified. We found that a 0.1 Å decrease of the Au-Au bond length could induce a blue-shift of 30 nm in the photoluminescence spectra of gold nanoclusters. From theoretical calculations, the origins of the blue shift and enhanced photoluminescence under pressure are investigated, which are ascribed to molecular orbital symmetry and conformational locking, respectively. The combination of the high-pressure *in-situ* X-ray results with both theoretical and experimental optical spectra provides a direct and generalizable avenue to unveil the underlying structure-property relations for nanoclusters and nanoparticles which cannot be obtained through traditional physical chemistry measurements.

Main Text: Nanoparticles have been widely used in sensing, diagnostics, and devices based on their excellent optical and electronic properties.[1–4] For a comprehensive understanding of the intriguing optical properties in nanoparticles, the ability to gradually modify nanoparticle structure at the atomic scale, while observing changes in their optical properties is edifying. This is hindered by the lack of atomic precision in nanoparticle synthesis and the heterogeneity of nanoparticle samples, which have been long-standing issues in nanochemistry.[1] Longstanding unsolved mechanisms of intriguing optical phenomena in nanoparticles, such as blinking behavior and dark states, has also been hampered. In the past decade, atomic-level precision has been partially realized in the synthesis of ultrasmall (1-2 nm in diameter) gold, silver, and copper nanoparticles (often called nanoclusters) which exhibit multiple excitonic absorption bands and bright near-infrared luminescence beyond 1000 nm with unique large Stokes shifts.[5–19] Single crystals of some nanoclusters were subsequently developed, and their atomic structures were directly determined by X-ray single-crystal diffraction analysis.[11,20–24] This provides the opportunity to investigate the atomic-level structure dependence of the optical[25,26], catalytic[27] and other properties in nanoclusters.

Unfortunately, the design, synthesis, structure determination, and measurement of novel nanoclusters is extremely time consuming. Researchers have modified existing gold nanoclusters through heating, etching, ligand exchange, and chemical transformations.[1,14,28] However, it is difficult to independently change structural parameters, such as the bond length and atomic connectivity, using traditional chemical or thermal modifications. Meanwhile, the measurement of dynamic changes can also be challenging in the event of rapid structural fluctuations.

Here, we conduct high-pressure single-crystal X-ray diffraction (XRD), combined with *in-situ* optical measurements and theoretical simulations in order to gain a deeper understanding of the atomic-level structure-property relationships of metal nanoclusters. High-pressure diamond anvil cells (DAC) are used to gradually vary the atomic structures of the nanoclusters in a way which cannot be realized by traditional chemistry. The X-ray and optical transparency of the diamond anvils allows the precise measurement of structural and chemical changes *in-situ* using diffraction and spectroscopic techniques.[29–32] This work adds to our previous high-pressure optical measurements[18,19,33] by using *in-situ* single-crystal XRD to directly and unambiguously identify the atomic-scale structural variation under pressure. This is extremely challenging, because nanoclusters single crystals generally have very large unit cells (normally bigger than ~4000 $Å^3$)

with low symmetry (normally triclinic or monoclinic). Solving their X-ray structures necessitates the acquisition of large numbers of the diffraction spots from a wide range of different directions, which is extremely difficult due to the limited opening angles of the DAC and the allowed scanning mode (only phi scans are available) of the high-pressure setup (Figure 1A).

To overcome these technical challenges, a recently developed DAC with a wide 120^0 opening angle was used. This has enabled to acquisition of sufficient diffraction spots at a wide range of angles. High quality single crystals of $[Au_{25}(S\text{-}PET)_{18}]^{-}TOA^{+}$ (S-PET = 2-phenylethylthiol; TOA = the tetraoctylamonium cation, abbreviated $Au_{25}S_{18}$ hereafter) were synthesized.[5,34,35] The unit cell consists of only one nanocluster (inset of Figure 1B), which is smaller than the unit cell of other single crystals of nanoclusters. In addition, the $Au_{25}S_{18}$ single crystals are stable under ambient laboratory conditions.[5,34,35]

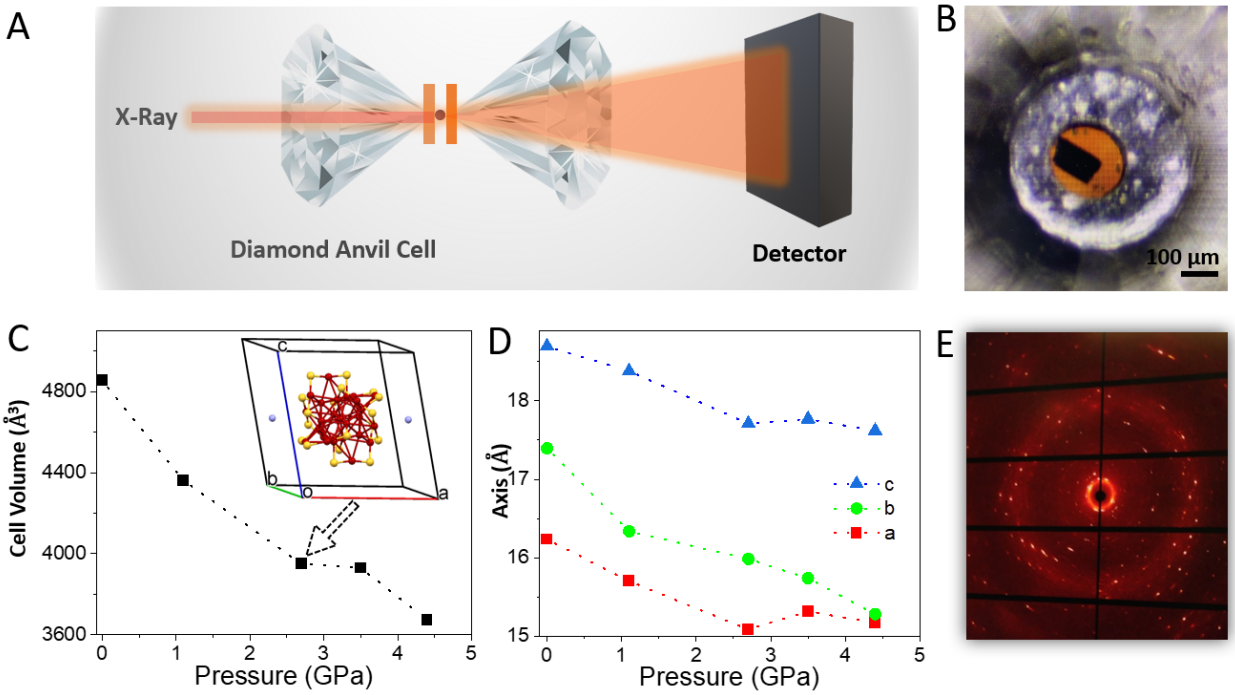

Figure 1. High-Pressure Single-Crystal XRD Study of $Au_{25}S_{18}$ Nanocluster. (A) Schematic of the experimental setup. (B) Optical image of a typical single crystal of $Au_{25}S_{18}$ in the DAC. (C) Experimental unit cell volume and (D) lattice parameters at increasing pressures. Inset of B is the experimentally determined structure of $Au_{25}S_{18}$ and its unit cell at 2.7 GPa. (E) Image of the X-ray diffraction spots of $Au_{25}S_{18}$ crystal at 0 GPa.

$Au_{25}S_{18}$ is composed of a Au_{13} icosahedral kernel protected by 6 Au_2S_3 surface motifs.[5,35] As shown in Figure 1C, the volume of the unit cell of the $Au_{25}S_{18}$ single crystal decreases by >24% at 4.4 GPa, with the largest change occurring over the first 2.7 GPa. The inset of Figure 1B is the

experimentally determined structure of $Au_{25}S_{18}$ and its unit cell at 2.7 GPa of applied pressure. The room-temperature bulk modulus for the $Au_{25}S_{18}$ nanocluster is calculated to be 16.7 GPa, based on the following equation: $K= -V\frac{dP}{dV}$,where P is pressure, V is the initial volume of the substance, and dP/dV denotes the derivative of pressure with respect to volume. All of the relative cell parameters under increasing pressures are shown in Figure 1D. It can be observed that the lengths of the a, b, and c axis of the unit cell continually decrease with increasing pressure. The a and c axis of the unit cell slightly increase at 3.5 GPa. The structure is compressed along the b axis slightly more than the other axes at the highest pressure.

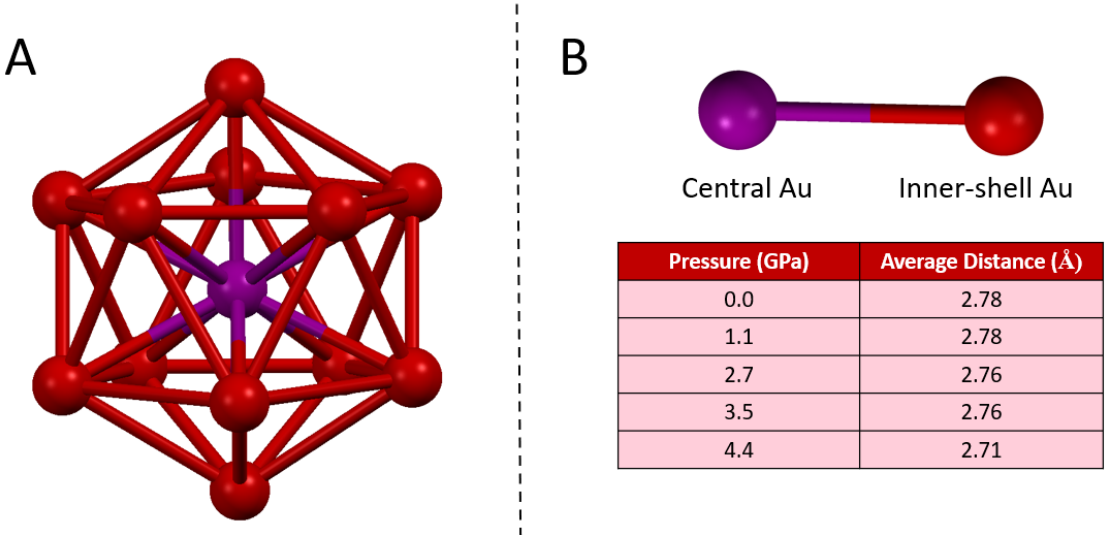

Pressure (GPa)	Average Distance (Å)
0.0	2.78
1.1	2.78
2.7	2.76
3.5	2.76
4.4	2.71

Figure 2. X-Ray Structure of $Au_{25}S_{18}$ Nanocluster under High-Pressure. (A) Resolved structure of the Au_{13} icosahedral kernel at 1.1 GPa. (central Au: purple; inner-shell Au: red) (B) The average distance between the central Au atom and the icosahedral inner-shell Au atoms at different pressures.

The atomic positions of all 25 Au and 18 S atoms of the $Au_{25}S_{18}$ nanocluster were experimentally defined (crystal and structural refinement data at 0, 1.1, 2.7, 3.5 and 4.4 GPa are included in the supporting information). **Figure 2A** shows the atomic structure of the Au_{13} icosahedral kernel of the Au_{25} under 1.1 GPa of pressure. Figure 2B shows the distances between the central Au atom (purple) and other 12 Au atoms (red) on the icosahedral inner-shell. The average Au-Au bond length contracts from 2.78 Å to 2.71 Å by increasing pressure to 4.4 GPa. Similarly, the bond distance between the 12 inner-shell Au atoms (red) contract from 2.92 Å to 2.83 Å on average as the pressure increases from 0 to 4.4 GPa.

These structural changes are compared to the pressure-dependent PL and absorption of $Au_{25}S_{18}$ (**Figure 3**). As with the high-pressure XRD experiment, 2-ethylcyclohexane was used as the quasi-hydrostatic pressure medium for the PL measurements. The PL blue-shifts and increases in intensity as the pressure increases to 2.8 GPa. As the pressure further increases from 2.8 GPa to 6.8 GPa, the PL position slightly blue-shifts and the intensity decreases. A similar blue-shift was observed in the absorption spectra. To obtain the pressure-dependent absorption spectra, nanoclusters were dispersed in toluene, which served as a non-hydrostatic pressure medium. The major absorption at ~ 680 nm blue-shifts as the pressure increases to ~ 1.8 GPa and then red shifts when the pressure increases from 1.8 to 2.6 GPa. This abrupt red-shift may arise from the freezing of toluene at ~2 GPa. For pressures above 2.6 GPa, the absorption shows negligible blue-shift. The similar pressure-dependence of the major absorption peak at ~680 nm and the PL peak at ~1000 nm indicate that their underlying electronic transitions are likely to be the same. The pressure-dependent optical changes for $Au_{25}S_{18}$ are also consistent with the pressure-dependent X-ray results in which contraction of the Au_{13} kernel occur under pressures up to 4.4 GPa.

These experimental findings were also corroborated by DFT simulations at a series of applied pressures which follow previously established methodology.[18,33,36] The results of DFT pressure simulations on the $Au_{25}S_{18}$ nanocluster are shown in Figure 3C and 3D. The major absorption band shows a general blue-shifting behavior (from 859 nm to 789 nm) with increasing pressure, with some resistance in the lower pressure region from 0.5 GPa to 1.0 GPa. Figure 3D shows how geometric changes in the Au-Au bond lengths associated with excited-state (S_1) relaxation (black) correlate with the pressure-induced structural changes between the range of 1.0 GPa and 2.5 GPa. The relaxed excited state geometry is asymmetric, giving rise to mild charge separation. This change in the electronic structure is shown via charge-difference densities (CDDs) in the inset of Figure 3D. Here, charge moves from blue to yellow areas of electron density in response to photoexcitation. The CDDs of $Au_{25}S_{18}$ at 0 GPa and 2.5 GPa of applied pressure are shown in the inset of Figure 3C. A more detailed account of the molecular orbitals (MOs) involved in these optical transitions can be found in the SI, along with gas-phase results.

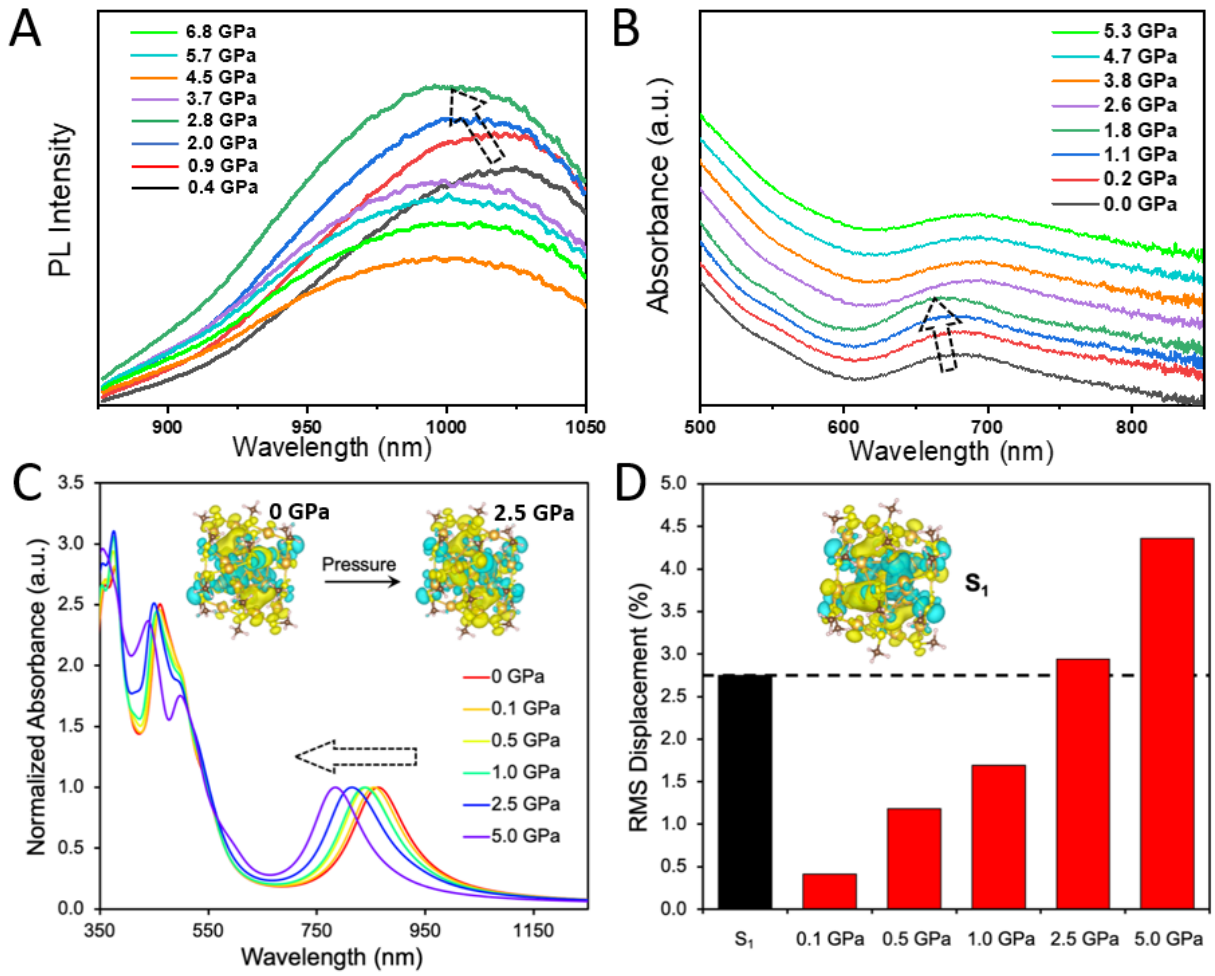

Figure 3. High-Pressure Optical Study and DFT Analysis of the $Au_{25}S_{18}$ Nanocluster. (A) Pressure-dependent PL spectra of the $Au_{25}S_{18}$ single-crystal. 2-ethylcyclohexane is chosen as the quasi-hydrostatic pressure medium. (B) Pressure-dependent absorption spectra of $Au_{25}S_{18}$ dissolved in toluene. The arrows denote the blue shift of the absorption peak at ~680 nm. (C) Pressure-dependent linear-response time-dependent DFT (TDDFT) excitation spectra where excitations were convoluted by Lorentzian functions (width = 0.1 eV). (D) Root mean square (RMS) displacement of Au-Au bond lengths as a percent of the equilibrium ground-state geometry for the relaxed excited state, S_1 (Black), and for structures under applied pressure (red). Insets show relevant charge-difference densities (CDDs) at (C) equilibrium of 0 GPa, high pressure of 2.5 GPa, and (D) the relaxed excited-state geometry.

The pressure-induced changes in each individual Au-Au bond length with a threshold of < 3.4 Å were carefully tracked throughout the pressure simulations and referenced to the equilibrated structure at ambient conditions. The root mean square (RMS) displacement from the optimal 0 GPa bond lengths as a function of pressure (red) are shown in Figure 3D. As expected, the RMS displacement increases with increasing pressure. The overarching trend from 0 GPa to 5.0 GPa is that bond lengths are contracting, which is consistent with the experimental high-pressure X-ray

results as shown in Figure 2. However, in many cases there are bonds that increase in length with increasing pressure. This is a result of contractions along one axis necessitating some expansion along an orthogonal axis, which can be observed experimentally in the change of the length of unit-cell axes “a” and “c” at 3.5 GPa (Figure 1C). Computationally, such an effect is noticeable from within small incremental pressure changes, but not after significant reduction in overall unit-cell volume.

The effects of asymmetric contraction are also evident in the CDD of S_1 (inset of Figure 3D), which shows how the electron-hole pair generated from photoexcitation changes due to geometric relaxation of the atomic coordinates in the gas phase. Here, electron density (yellow orbitals) shifts to one side of the outer shell of the Au_{13} core, yielding mild charge-transfer (CT) character. This electron-hole distribution is assumed to correspond to the origins of PL, and the RMS displacement of the Au-Au bond lengths after excited-state relaxation are shown by the black column in Figure 3D. Of particular interest is that the electron-hole distribution of relaxed S_1 (Figure 3D inset) shows similar CT character to the CDD of S_1 with 2.5 GPa of applied pressure (Figure 3C inset). Moreover, the structural changes associated with excited state relaxation fall close to what was found for 2.5 GPa (dashed black line). This correlates with the pressure of 2.8 GPa at which the measured PL intensity reaches a maximum (Figure 3A).

High-pressure optical studies were also conducted on another icosahedral Au nanocluster, the rod-shaped Au_{25} (referred to as Au_{25}-R hereafter), which shows similar pressure characteristics. The atomic structure of the Au_{25}-R is shown in **Figure 4**. Figure 4B displays the pressure-dependent absorption spectra from 0 to 6.2 GPa in toluene (non-hydrostatic). It can be observed that the absorption peak at 680 nm blue-shifts to 670 nm as the pressure increases from 0 to 1.5 GPa. No significant blue-shift is observed as the pressure further increases from 1.5 to 3.1 GPa. From 3.1 to 6.2 GPa, the absorption blue-shifts again to ~ 650 nm. Figure 4C shows the pressure-dependent PL spectra from 0 to 6.2 GPa. It can be observed that from 0 to 1.5 GPa, the PL blue shifts in a similar fashion to the 680 nm absorption. As the pressure increase from 1.5 to 3.1 GPa, the PL slightly red-shifts; And from 3.1 to 6.2 GPa, the PL of Au_{25}-R blue-shifts again. The highest PL intensity occurs at 0.9 GPa. Figure S1 displays the pressure-dependent PL spectra of a Au_{25}-R single-crystal using 2-ethylcyclohexane as the pressure medium. It can be observed that the pressure-dependence of the PL of Au_{25}-R in the quasi-hydrostatic (2-ethylcyclohexane) medium is similar to non-hydrostatic (toluene) conditions.

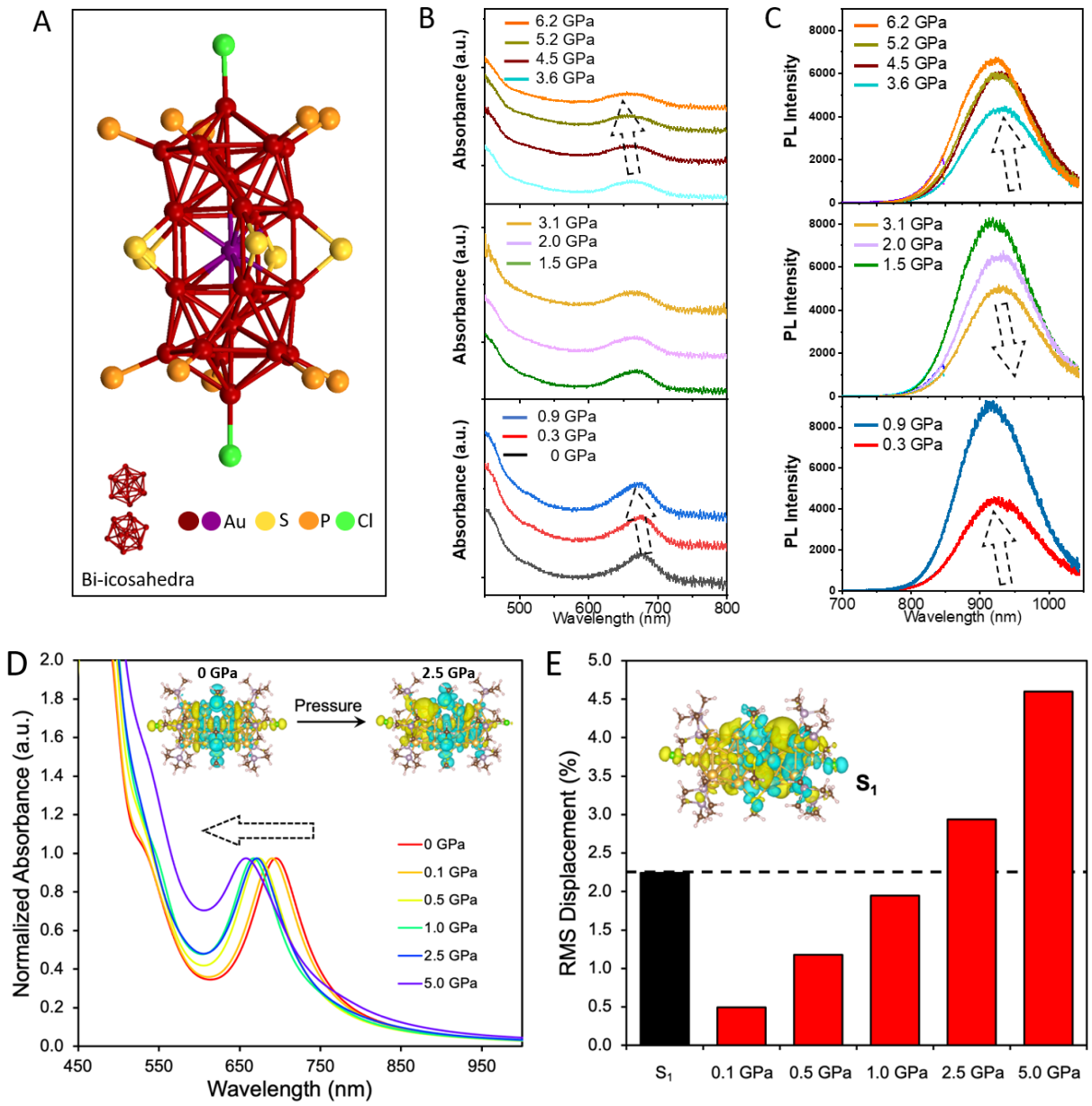

Figure 4. High-Pressure Optical Study and DFT Analysis of Rod-Shaped Au_{25}. (A) Atomic structure of Au_{25} nanorod.[37] Red/Purple = Au; yellow = S; Dark yellow=P; Carbon tails are omitted for clarity. (B) Pressure-dependent absorption spectra of Au_{25} nanorod. (C) Pressure-dependent PL spectra of Au_{25} nanorod. The arrows denote the blue and red shift of the absorption peak at ~680. (C) Pressure-dependent TDDFT excitation spectra where excitations were convoluted by Lorentzian functions. (D) RMS displacement of Au-Au bond lengths as a percent of the equilibrium ground-state geometry for the relaxed excited state, S_1 (black), and for structures under applied pressure (red). Insets show relevant CDDs at (D) equilibrium of 0 GPa, high pressure of 2.5 GPa, and (E) the relaxed excited-state S_1 geometry.

DFT simulations for the Au_{25}-R nanocluster are shown in Figure 4D and 4E. Here, the characteristic absorption band shifts from 695 nm to 657 nm as pressure is increased to 5.0 GPa.

For reference, the calculated gas-phase absorption spectrum is given in the SI. An interesting note from the results of these simulations is that the blue-shift is not a totally smooth transition, but faces resistance in the 1.0 GPa to 2.5 GPa range. In fact, there is a marginal red-shift by a few nanometers. The inset of Figure 4D shows the CDDs of the lowest lying singlet excited state at 0 GPa and 2.5 GPa of applied pressure. Similar to the spherical nanocluster, $Au_{25}S_{18}$, it can be seen that under ambient conditions the excited state nanocluster shows centrosymmetric electron density redistribution, with core-to-shell character. This finding is consistent with previously reported results. Again, due to some asymmetric compression of the rod-like nanocluster, the CDD at 2.5 GPa displays CT character, with electron density moving towards one end of the rod. However, unlike $Au_{25}S_{18}$ the characteristic absorption band at 695 nm for Au_{25}-R calculated under ambient conditions does not correspond to the lowest lying excited state (S_1), but instead a higher-ordered excitation (c. S_{10}) and is not assumed to be the origin of PL for this species. The characteristic absorption band does not correspond to the same luminescent state giving rise to emission in Figure 4C. This is further corroborated by opposing trends in the absorption spectra and PL spectra as a function of pressure. These effects were discussed at length in previous work.[18]

To understand how pressure induces the observed changes in both spherical and rod-like Au_{25}, relevant MOs that comprise the optically-active excited states in Figures 3C and 4D are given in the SI. The pressure-dependence of a given MO's energy level is governed by its bonding or antibonding character, where the energy of bonding MOs trend downward when the atomic coordinates are compressed and the energy of antibonding MOs trend upward. In the case of $Au_{25}S_{18}$ (Figure S5), all low-energy excited states (~S_1 through S_{10}) are comprised of mixed 1-electron transitions from predominantly bonding MOs to predominantly anti-bonding MOs. Ultimately, this leads to universal blue-shifting behavior in the optical spectra. This is a unique property of nanoclusters featuring a highly symmetric icosahedral core, whereas previously studied nanoclusters[33] that exhibit red-shifting behavior under pressure do not display clear bonding-to-antibonding transition. In the case of Au_{25}-R, the lowest-lying excited state (S_1) is a dark state, as previously reported,[17] that is a purely HOMO-LUMO transition (Table S1). Along the long axis of the nanorod, the HOMO is bonding and the LUMO is antibonding, whereas along the azimuthal axis the HOMO is antibonding and the LUMO is bonding (Figure S9). As such, chromic shifts in the optical spectra depend on the relative contraction of the individual crystal axes. By examining single clusters extracted from the simulated crystal structures in Figure S8, it

was found that the long axis of the nanorod contracts the most from 0 GPa to 1.0 GPa (-3.2% in end-to-end distance) and from 2.5 GPa to 5.0 GPa (additional -2.5% in end-to-end distance) where blue-shifting PL dominates. Alternatively, the circumference of the nanorod does not show appreciable contraction until pressures are beyond 1.0 GPa, which causes red-shifting behavior. The interplay between these two effects gives rise to S_1 shifting from 1.398 eV at 0 GPa to 1.471 eV at 1.0 GPa, before reversing to 1.424 eV at 5.0 GPa. These results confirm the possibility of anisotropic compression leading to color tunability.

Although the emissive excited state (S_1) for these icosahedral nanoclusters exhibits low or negligible oscillator strengths in their native equilibrium geometry (Table S1), geometry relaxations of S_1 (the photoluminescent geometry, inset of Figure 3D and 4E) gave rise to significant enhancements ($f > 0.2$). The large Stokes shift that is characteristic of these two gold nanoclusters featuring icosahedral cores is attributed to this activation of otherwise *dark* states after structural relaxation. A natural assumption would be that if the geometry of these nanoclusters could be constrained to a configuration reminiscent of the relaxed S_1 geometry, the PL intensity could be maximized. As indicated in Figures 3D and 4E, the overall change in Au-Au bond lengths for both nanoclusters correlates with the change observed from S_1 relaxation in the region between 1.0 GPa and 2.5 GPa. Moreover, the electronic structure (Insets, Figures 3C and 3D, Figure 4D and 4E) in this pressure regime also correlates with that of the relaxed excited state. Indeed, the calculated oscillator strength of S_1 for both nanoclusters were found to increase with pressure up to 2.5 GPa before decreasing again. Such an effect is seen in the pressure-dependent PL spectra in Figures 3A and 4C. These results show that pressure can act as a "conformational lock" that constrains the nanocluster to the photoluminescent geometry at intermediate pressures, further activating the dark states and ultimately enhancing PL intensity. Notably, the gold nanoclusters with icosahedral motifs discussed here all feature this inversion symmetry and, in turn, lowest-energy dark states. Such states in other semiconducting materials, including perovskites and tungsten disulfide, have been probed by two-photon and magneto-PL spectroscopy to reveal minimal optical activity in the ground-state geometry.[38,39] In this work, these dark states have been shown to contribute to PL when structural relaxation in the excited state is accounted for, indicating the need for pressure-dependent spectroscopic studies in other fields.

Overall, this study represents the first example of a high-pressure single-crystal X-ray diffraction analysis of nanoparticles. The pressure-dependent sub-angstrom structural evolution of

a gold nanocluster has been directly identified and correlated with the blue-shifts of the optical transitions, indicating that the subtle changes of the kernel structure could induce the significant difference in the optical properties of gold nanoclusters. Structural changes were corroborated by DFT simulations, which related MO symmetry to the observed chromic shifts in electronic spectra and geometric constraints to enhanced PL intensity. The origin of the unique and bright near-infrared PL beyond 1000 nm in icosahedral gold nanoclusters were revealed to be the activation of dark states after excitation, which can be further promoted by high pressure. We envision that the high-pressure framework developed in this work can be used to study the underlying photophysics and structure-property relations of other optical nanomaterials.

Acknowledgements: We greatly thank Prof. Shuxin Wang for proving single crystals of Au_{25} for the preliminary test. Q.L., X.W.G., C.J.Z., and G.C.S. acknowledge National Science Foundation (NSF) grant DMR-2002936/2002891. Part of this work was performed at the Stanford Nano Shared Facilities (SNSF), which is supported by the National Science Foundation under award ECCS-1542152. C.J.Z., and G.C.S. were supported by DOE grant DE-AC02-06CH11357 for theory development. This research used resources of the Advanced Light Source, a U.S. DOE Office of Science User Facility under contract no. DE-AC02-05CH11231.This research was supported in part through the computational resources and staff contributions provided for the Quest high-performance computing facility at Northwestern University which is jointly supported by the Office of the Provost, the Office for Research, and Northwestern University Information Technology.

Author Contributions: Q.L. and X.W.G. conceived the idea and supervised the research of this work. Q.L. synthesized the nanocrystals. Q.L., B.K., A.P.; M.K., G.S.; D.D., A.L. and J.K. performed the high-pressure XRD. K.K., C.G.G.; Q.L., B.K., performed the single-crystal XRD analysis. C.J.Z. and G.C.S. performed the DFT simulations and analysis. Q.L., X.W.G., C.J.Z. and G.C.S. wrote the manuscript. All authors have given approval to the final version of the manuscript.

Competing Interests: The authors declare no competing financial interest.

References

(1) Jin, R.; Zeng, C.; Zhou, M.; Chen, Y. Atomically Precise Colloidal Metal Nanoclusters and Nanoparticles: Fundamentals and Opportunities. *Chem. Rev.* **2016**, *116* (18), 10346–10413.

(2) Boles, M. A.; Engel, M.; Talapin, D. V. Self-Assembly of Colloidal Nanocrystals: From Intricate Structures to Functional Materials. *Chem. Rev.* **2016**, *116* (18), 11220–11289.

(3) Dykman, L.; Khlebtsov, N. Gold Nanoparticles in Biomedical Applications: Recent Advances and Perspectives. *Chem. Soc. Rev.* **2012**, *41* (6), 2256–2282.
(4) Jing, L.; Kershaw, S. V.; Li, Y.; Huang, X.; Li, Y.; Rogach, A. L.; Gao, M. Aqueous Based Semiconductor Nanocrystals. *Chem. Rev.* **2016**, *116* (18), 10623–10730. https://doi.org/10.1021/acs.chemrev.6b00041.
(5) Zhu, M.; Aikens, C. M.; Hollander, F. J.; Schatz, G. C.; Jin, R. Correlating the Crystal Structure of A Thiol-Protected Au25 Cluster and Optical Properties. *J. Am. Chem. Soc.* **2008**, *130* (18), 5883–5885.
(6) Akola, J.; Walter, M.; Whetten, R. L.; Häkkinen, H.; Grönbeck, H. On the Structure of Thiolate-Protected Au25. *J. Am. Chem. Soc.* **2008**, *130* (12), 3756–3757.
(7) Dass, A.; Stevenson, A.; Dubay, G. R.; Tracy, J. B.; Murray, R. W. Nanoparticle MALDI-TOF Mass Spectrometry without Fragmentation: Au25(SCH2CH2Ph)18 and Mixed Monolayer Au25(SCH2CH2Ph)18−x(L)x. *J. Am. Chem. Soc.* **2008**, *130* (18), 5940–5946.
(8) Azubel, M.; Koivisto, J.; Malola, S.; Bushnell, D.; Hura, G. L.; Koh, A. L.; Tsunoyama, H.; Tsukuda, T.; Pettersson, M.; Häkkinen, H.; Kornberg, R. D. Electron Microscopy of Gold Nanoparticles at Atomic Resolution. *Science* **2014**, *345* (6199), 909–912.
(9) Jadzinsky, P. D.; Calero, G.; Ackerson, C. J.; Bushnell, D. A.; Kornberg, R. D. Structure of a Thiol Monolayer-Protected Gold Nanoparticle at 1.1 Å Resolution. *Science* **2007**, *318* (5849), 430–433.
(10) Zeng, C.; Qian, H.; Li, T.; Li, G.; Rosi, N. L.; Yoon, B.; Barnett, R. N.; Whetten, R. L.; Landman, U.; Jin, R. Total Structure and Electronic Properties of the Gold Nanocrystal Au36(SR)24. *Angewandte Chemie* **2012**, *124* (52), 13291–13295.
(11) Zeng, C.; Chen, Y.; Kirschbaum, K.; Appavoo, K.; Sfeir, M. Y.; Jin, R. Structural Patterns at All Scales in a Nonmetallic Chiral Au133(SR)52 Nanoparticle. *Science Advances* **2015**, *1* (2), e1500045.
(12) Pyo, K.; Thanthirige, V. D.; Kwak, K.; Pandurangan, P.; Ramakrishna, G.; Lee, D. Ultrabright Luminescence from Gold Nanoclusters: Rigidifying the Au(I)–Thiolate Shell. *J. Am. Chem. Soc.* **2015**, *137* (25), 8244–8250.(13) Liu, H.; Hong, G.; Luo, Z.; Chen, J.; Chang, J.; Gong, M.; He, H.; Yang, J.; Yuan, X.; Li, L.; Mu, X.; Wang, J.; Mi, W.; Luo, J.; Xie, J.; Zhang, X.-D. Atomic-Precision Gold Clusters for NIR-II Imaging. *Advanced Materials* **2019**, *31* (46), 1901015.
(14) Chakraborty, I.; Pradeep, T. Atomically Precise Clusters of Noble Metals: Emerging Link between Atoms and Nanoparticles. *Chem. Rev.* **2017**, *117* (12), 8208–8271.
(15) Takano, S.; Tsukuda, T. Chemically Modified Gold/Silver Superatoms as Artificial Elements at Nanoscale: Design Principles and Synthesis Challenges. *J. Am. Chem. Soc.* **2021**, *143* (4), 1683–1698.
(16) Narouz, M. R.; Takano, S.; Lummis, P. A.; Levchenko, T. I.; Nazemi, A.; Kaappa, S.; Malola, S.; Yousefalizadeh, G.; Calhoun, L. A.; Stamplecoskie, K. G.; Häkkinen, H.; Tsukuda, T.; Crudden, C. M. Robust, Highly Luminescent Au13 Superatoms Protected by N-Heterocyclic Carbenes. *J. Am. Chem. Soc.* **2019**, *141* (38), 14997–15002.
(17) Li, Q.; Zeman, C. J.; Ma, Z.; Schatz, G. C.; Gu, X. W. Bright NIR-II Photoluminescence in Rod-Shaped Icosahedral Gold Nanoclusters. *Small* **2021**, *17* (11), 2007992.
(18) Li, Q.; Zeman, C. J.; Schatz, G. C.; Gu, X. W. Source of Bright Near-Infrared Luminescence in Gold Nanoclusters. *ACS Nano* **2021**, *15* (10), 16095–16105.
(19) Li, Q.; Zhou, D.; Chai, J.; So, W. Y.; Cai, T.; Li, M.; Peteanu, L. A.; Chen, O.; Cotlet, M.; Wendy Gu, X.; Zhu, H.; Jin, R. Structural Distortion and Electron Redistribution in Dual-Emitting Gold Nanoclusters. *Nature Communications* **2020**, *11* (1), 2897.
(20) Yang, H.; Wang, Y.; Chen, X.; Zhao, X.; Gu, L.; Huang, H.; Yan, J.; Xu, C.; Li, G.; Wu, J.; Edwards, A. J.; Dittrich, B.; Tang, Z.; Wang, D.; Lehtovaara, L.; Häkkinen, H.; Zheng, N. Plasmonic Twinned Silver Nanoparticles with Molecular Precision. *Nat Commun* **2016**, *7* (1), 1–8. (21)Tian, S.; Li, Y.-Z.; Li, M.-B.; Yuan, J.; Yang, J.; Wu, Z.; Jin, R. Structural Isomerism in Gold Nanoparticles Revealed by X-Ray Crystallography. *Nature Communications* **2015**, *6* (1), 8667.

(22) Yan, N.; Xia, N.; Liao, L.; Zhu, M.; Jin, F.; Jin, R.; Wu, Z. Unraveling the Long-Pursued Au144 Structure by x-Ray Crystallography. *Science Advances* **2018**, *4* (10), eaat7259.
(23) Tang, L.; Ma, A.; Zhang, C.; Liu, X.; Jin, R.; Wang, S. Total Structure of Bimetallic Core–Shell [Au42Cd40(SR)52]2− Nanocluster and Its Implications. *Angewandte Chemie* **2021**, *133* (33), 18113–18117.
(24) Ghosh, A.; Huang, R.-W.; Alamer, B.; Abou-Hamad, E.; Hedhili, M. N.; Mohammed, O. F.; Bakr, O. M. [Cu61(StBu)26S6Cl6H14]+: A Core–Shell Superatom Nanocluster with a Quasi-J36 Cu19 Core and an "18-Crown-6" Metal-Sulfide-like Stabilizing Belt. *ACS Materials Lett.* **2019**, *1* (3), 297–302.
(25) Higaki, T.; Zhou, M.; Lambright, K. J.; Kirschbaum, K.; Sfeir, M. Y.; Jin, R. Sharp Transition from Nonmetallic Au246 to Metallic Au279 with Nascent Surface Plasmon Resonance. *J. Am. Chem. Soc.* **2018**, *140* (17), 5691–5695.
(26) Zhou, M.; Jin, R.; Sfeir, M. Y.; Chen, Y.; Song, Y.; Jin, R. Electron Localization in Rod-Shaped Triicosahedral Gold Nanocluster. *PNAS* **2017**, *114* (24), E4697–E4705.
(27) Cai, X.; Saranya, G.; Shen, K.; Chen, M.; Si, R.; Ding, W.; Zhu, Y. Reversible Switching of Catalytic Activity by Shuttling an Atom into and out of Gold Nanoclusters. *Angewandte Chemie International Edition* **2019**, *58* (29), 9964–9968.
(28) Li, Q.; Luo, T.-Y.; Taylor, M. G.; Wang, S.; Zhu, X.; Song, Y.; Mpourmpakis, G.; Rosi, N. L.; Jin, R. Molecular "Surgery" on a 23-Gold-Atom Nanoparticle. *Science Advances* **2017**, *3* (5), e1603193.
(29) Mao, H.-K.; Chen, X.-J.; Ding, Y.; Li, B.; Wang, L. Solids, Liquids, and Gases under High Pressure. *Rev. Mod. Phys.* **2018**, *90* (1), 015007.
(30) Zhang, L.; Wang, Y.; Lv, J.; Ma, Y. Materials Discovery at High Pressures. *Nature Reviews Materials* **2017**, *2* (4), 17005.
(31) Bai, F.; Bian, K.; Huang, X.; Wang, Z.; Fan, H. Pressure Induced Nanoparticle Phase Behavior, Property, and Applications. *Chem. Rev.* **2019**, *119* (12), 7673–7717.
(32) Xiao, G.; Cao, Y.; Qi, G.; Wang, L.; Liu, C.; Ma, Z.; Yang, X.; Sui, Y.; Zheng, W.; Zou, B. Pressure Effects on Structure and Optical Properties in Cesium Lead Bromide Perovskite Nanocrystals. *J. Am. Chem. Soc.* **2017**, *139* (29), 10087–10094.
(33) Li, Q.; Mosquera, M. A.; Jones, L. O.; Parakh, A.; Chai, J.; Jin, R.; Schatz, G. C.; Gu, X. W. Pressure-Induced Optical Transitions in Metal Nanoclusters. *ACS Nano* **2020**, *14* (9), 11888–11896.
(34) Wu, Z.; Suhan, J.; Jin, R. One-Pot Synthesis of Atomically Monodisperse, Thiol-Functionalized Au25 Nanoclusters. *J. Mater. Chem.* **2009**, *19* (5), 622–626.
(35) Heaven, M. W.; Dass, A.; White, P. S.; Holt, K. M.; Murray, R. W. Crystal Structure of the Gold Nanoparticle [N(C8H17)4][Au25(SCH2CH2Ph)18]. *J. Am. Chem. Soc.* **2008**, *130* (12), 3754–3755.
(36) Li, D.; Liu, Q.; Qi, Q.; Shi, H.; Hsu, E.-C.; Chen, W.; Yuan, W.; Wu, Y.; Lin, S.; Zeng, Y.; Xiao, Z.; Xu, L.; Zhang, Y.; Stoyanova, T.; Jia, W.; Cheng, Z. Gold Nanoclusters for NIR-II Fluorescence Imaging of Bones. *Small* **2020**, *16* (43), 2003851.
(37) Shichibu, Y.; Negishi, Y.; Watanabe, T.; Chaki, N. K.; Kawaguchi, H.; Tsukuda, T. Biicosahedral Gold Clusters [Au25(PPh3)10(SCnH2n+1)5Cl2]2+ (n = 2−18): A Stepping Stone to Cluster-Assembled Materials. *J. Phys. Chem. C* **2007**, *111* (22), 7845–7847.
(38) Tamarat, P.; Bodnarchuk, M. I.; Trebbia, J.-B.; Erni, R.; Kovalenko, M. V.; Even, J.; Lounis, B. The Ground Exciton State of Formamidinium Lead Bromide Perovskite Nanocrystals Is a Singlet Dark State. *Nat. Mater.* **2019**, *18* (7), 717–724.
(39) Ye, Z.; Cao, T.; O'Brien, K.; Zhu, H.; Yin, X.; Wang, Y.; Louie, S. G.; Zhang, X. Probing Excitonic Dark States in Single-Layer Tungsten Disulphide. *Nature* **2014**, *513* (7517), 214–218.

Supporting Information

Experimental, computational methods, more computational results and author contributions are in the Supporting Information.